Polymer Degradation and Stability 154 (2018) 27–36

Contents lists available at ScienceDirect

Polymer Degradation and Stability

journal homepage: www.elsevier.com/locate/polydegstab

Improving fire safety of epoxy filled with graphene hybrid incorporated with zeolitic imidazolate framework/layered double hydroxide

Wenzong Xu*, Xiaoling Wang, Yucheng Liu, Wu Li, Rui Chen

School of Materials Science and Chemical Engineering, Anhui Jianzhu University, 292 Ziyun Road, Hefei, Anhui, 230601, People's Republic of China

ARTICLE INFO

Article history:
Received 13 March 2018
Received in revised form
5 May 2018
Accepted 20 May 2018
Available online 23 May 2018

Keywords:
Hybrid composites
Graphene
Layered structures
Flame retardant
Smoke suppression

ABSTRACT

In this work, a novel graphene (RGO) hybrid added with Zeolitic Imidazolate Framework/Layered Double Hydroxide (ZIF/LDH) was prepared to obtain a synergistic system (RGO-LDH/ZIF-67). Subsequently, RGO-LDH/ZIF-67 was mixed into epoxy resin (EP) by physical blending for the purpose of improving its fire safety. Based on a series of tests and analyses, it was found that RGO-LDH/ZIF-67 was beneficial to reducing the heat release of EP during its burning process. The peak heat release rate (PHRR) and total heat release (THR) of the composite with 2 wt% RGO-LDH/ZIF-67 were reduced to 464 kW m^{-2} and 37.9 MJ m^{-2}, respectively. Simultaneously, the smoke production in its flame and flameless combustion were also reduced significantly. According to the char analysis of different composites, the main mechanism is discussed. This work provided a new type of modified RGO for improving the fire safety of EP.

1. Introduction

EP is broadly applied in the military and civil fields due to its outstanding mechanical properties, electrical insulation, chemical stability and excellent thermal properties [1–3]. However, EP is liable to combust in air, and a lot of toxic gas and smoke which endanger people's lives will be released during its combustion process, and, consequently, the application of EP is limited to some extent. In order to expand the application of EP, it is imperative to reduce its fire risk.

In recent years, more and more researchers have found that some carbon materials such as carbon nanotubes, expandable graphite and RGO can be applied for reducing the fire risk of EP [4–6]. Among those materials, RGO shows a flake structure of six-angle honeycomb lattice composed of sp^2 hybrid orbital by carbon atoms. It has received close attention because of its special two-dimensional nanostructures, and unique physical and chemical properties [7]. Recently, there have been increasing applications of RGO as an additive agent to reduce the fire hazard of polymers [8,9]. New findings indicate that RGO still has good thermal stability even when it is exposed to flame, and it shows a good flame retardant ability for polymers, and because of the obstruction of RGO, which can effectively retard the heat transmission and volatilization of combustible gas, so as to protect the substrate, preventing the further combustion of polymers [10,11]. Nevertheless, RGO tends to agglomerate because of the existence of Vander Waals' force, which makes it difficult to be dispersed well in composites. For the purpose of surmounting this defect, much work has been done on the surface modification of RGO, and some results have shown that the agglomeration of RGO has been significantly reduced after surface modification [12,13]. Specifically, there have also been some reports about the modification of RGO with layered double hydroxides (LDHs) [14].

LDHs show good thermal stability and excellent flame retardant performance. They have gradually become a focus in the field of flame retardants. It is due mainly to the fact that LDH can provide a physical barrier effect which can prevent the evaporation of flammable gas and oxygen during the burning of EP. Furthermore, the metal oxides generated in the burning process of LDH can promote the formation of carbon residue, and make a contribution in strengthening the barrier effect. At the same time, the water vapor generated during the decomposition process of LDH will absorb heat, and reduce the temperature of composite materials' surface, thereby playing a better role in retarding the combustion of polymer [15]. In addition, there is a certain amount of positive charges

* Corresponding author.
E-mail address: wengzongxu@ahjzu.edu.cn (W. Xu).

https://doi.org/10.1016/j.polymdegradstab.2018.05.022
0141-3910/

on LDH, which facilitates the surface modification of LDH. Despite numerous reports about surface modification of LDH, there have been few reports about the modification of LDH surface by metal organic frameworks (MOFs). In view of that, this research has been undertaken.

MOFs is a kind of crystalline porous material containing interconnected forms of periodic network structure, synthesized by self-assembly reaction between inorganic metal (metal ions or metal clusters) and organic ligands. It has attracted more and more attention because of its special structure and excellent performance, especially in the field of adsorption [16–18]. However, relatively few studies have been performed on the application of MOFs as an additive agent to reduce the fire risk of polymers. There are many kinds of MOFs, such as Isoreticular metal-organic frameworks (IRMOFs), zeoliticimidazolate frameworks (ZIFs), metarial sofistitute Lavoisierframeworks (MILs) and ocket-channel frameworks (PCNs). In particular, ZIF-67, as a kind of ZIFs, is synthesized based on cobalt ions and 2-methylimidazole, containing flame retardant elements of Co and N, and the metal oxide (Co_3O_4) generated during its combustion process has a catalytic effect which facilitates the generation of a dense char layer to prevent the substrate from further burning, and thus to accomplish the aim of reducing fire risk. Therefore, ZIF-67 was selected in this work to further reduce the fire hazard of polymer.

To our knowledge, a flame retardant with a single component can decrease the fire risk of composite materials when the amount of additive is large, but its flame retardant efficiency is rather low. However, a flame retardant containing more than one component would form a synergetic system, so as to better reduce the fire hazard [19,20]. Therefore, in this study, dual modification of RGO (RGO-LDH/ZIF-67) was performed by connecting RGO, LDH and ZIF-67 (as shown in Scheme 1). The morphology of the prepared flame retardants was studied. Subsequently, RGO-LDH/ZIF-67 was added into EP through physical blending. The effects of RGO-LDH/ZIF-67 on reducing the fire risk of EP were studied, and their main mechanism was also investigated.

2. Experimental

2.1. Materials

H_2SO_4 (98%), Graphite powder (spectral purity), $NaNO_3$, $KMnO_4$, HCl (37%), H_2O_2 (30%), H_2N_2 (80%), NaOH, ethyl alcohol, cobalt nitrate, 2-methylimidazole, absolute methanol, magnesium nitrate, aluminum nitrate, sodium carbonate anhydrous were bought from Shanghai Jutai Special Reagent Co., Ltd. (China). Epoxy resin (E-44) was bought from Wuxi Borui Chemical Technology Co., Ltd. (China). 3,3′-Dichloro-4,4′- diaminodiphenylmethane (MOCA) was bought from Shandong Guangxun Chemical Co., Ltd. (China).

2.2. Fabrication of flame retardants

2.2.1. Fabrication of RGO-LDH

GO was made with modified Hummer's method [21]. RGO-LDH was fabricated with a simple coprecipitation method as follows: Firstly, 0.32 g GO was dissolved in 100 ml deionized water, with addition of some sodium hydroxide and anhydrous sodium carbonate, and ultrasonic reaction for 1.5 h; the obtained homogeneous solution was poured into a 500 ml flask. Subsequently, magnesium nitrate (1.28 g) and aluminum nitrate (1.88 g) were dissolved completely in 200 ml water to obtain an uniform system, and this uniform liquor was added into the dispersion of GO by dropping. This system was adjusted to a PH of 10, and stirred for 24 h at 60 °C. Then hydrazine hydrate solution (0.75 ml) was added into the above system and its temperature was increased to 100 °C. The system was cooled down to room temperature after stirring for 2 h, washed repeatedly, and freeze dried to obtain RGO-LDH. RGO and MgAl-LDH were also obtained in the same way.

2.2.2. Fabrication of RGO-LDH/ZIF-67

RGO-LDH/ZIF-67 was fabricated with a simple process in the following steps: RGO-LDH (1 g) was ultrasonically dispersed in an appropriate amount of deionized water to acquire a homogeneous system (A), and 6.56 g 2-methylimidazole was dissolved in 100 ml

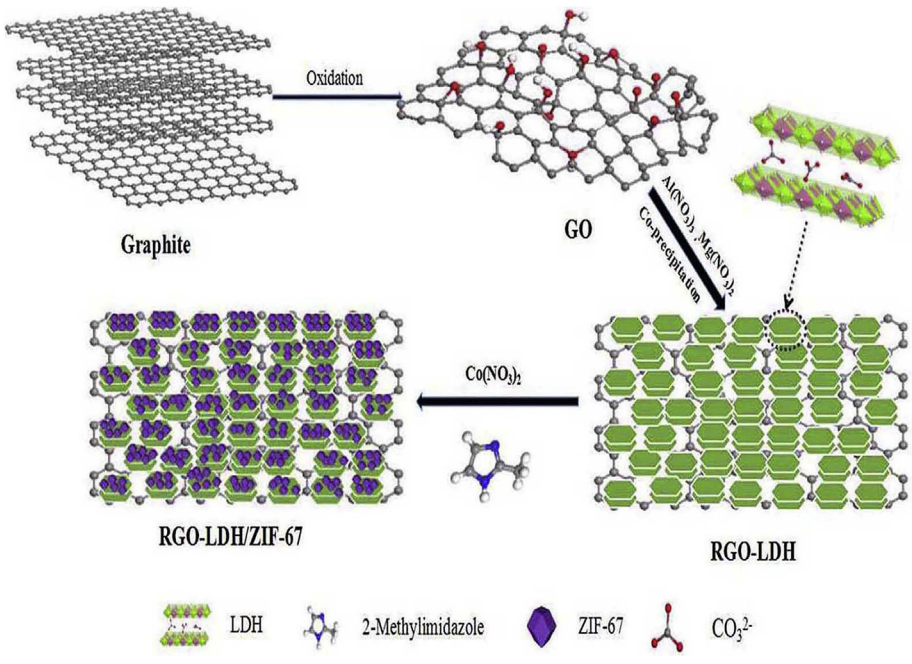

Scheme 1. Illustration of ZIF-67 modification of RGO-LDH.

anhydrous methanol to acquire a system B. Subsequently, the system B was dropped into the homogeneous solution A, and stirred for 6 h at room temperature. Then 4.98 g cobalt nitrate was dissolved in 100 ml anhydrous methanol and dropped into the above system, which underwent stirring for 24 h. Finally, the sediment was washed repeatedly and freeze dried to obtain RGO-LDH/ZIF-67.

2.3. Fabrication of different composites

Different composites were fabricated in a simple way. Taking the preparation of EP-RGO-LDH/ZIF-67 composite for example: Firstly, a certain amount of RGO-LDH/ZIF-67 was dissolved in a small amount of acetone solution for ultrasonic reaction until a uniform solution was formed. The above solution was then added into a certain amount of epoxy resin and strong stirring took place under the condition of 75 °C until a uniform system was formed. Subsequently, MOCA was melted at 120 °C and added into the above system for stirring until the formation of a homogeneous mixture. The above mixture was poured into a Teflon mold to sit for a period of time before curing at 110 °C for 2 h and 150 °C for 3 h continuously. The EP composite was prepared as a result (the specific formula was displayed in Table 1). All composites were fabricated in the same way.

2.4. Characterization

Fourier transform infrared spectroscopy (FTIR) was performed with Nicolet 6700 spectrometer (Nicolet Instrument Co., U.S.) with the KBr pellet technique. X-ray diffraction (XRD) analysis was made with XRD-7000 (Shimadzu, Japan) at a scanning speed of $2^\circ \cdot min^{-1}$ and a diffraction angle range of 5–60°. Raman spectra were obtained at room temperature by using a SPEX-1403 laser Raman spectrometer (SPEX Co., U.S.) with a back-scattering geometry and a wave length of 514.5 nm. Transmission electron microscope-energy-dispersive X-ray spectroscopic (TEM-EDS) measurements were conducted by using a JEOL-2010 instrument (JEOL Co., Japan) at an acceleration voltage of 200 kV. Thermogravimetric analysis (TGA) was performed with STA7200 (TA, Germany) in both air and nitrogen atmosphere with the heating rate of $20\ ^\circ C \cdot min^{-1}$, and a range of specimen mass from 6 to 10 mg. Differential scanning calorimetry (DSC) analysis was conducted by a DSC Q20 apparatus (TA, U.S.) with a heating rate of $10\ ^\circ C \cdot min^{-1}$ and a test temperature range from 50 to 145 °C. Limited oxygen index (LOI) values were measured on the basis of the standard procedure of ASTM D2863-2012 with an HC-2 oxygen index meter (China), and a sample size of $100 \times 10 \times 3\ mm^3$. Cone calorimetry test was carried out with a cone calorimeter (Nanjing Jiangning Analytical Instrument Company, China) on the basis of the ISO5660-1: 2002 standard. The size of the sample was $100 \times 100 \times 3\ mm^3$ and the thermal radiation was 25 kW m^{-2}. Smoke density was tested by using a JSC-2 smoke density meter (Nanjing Jiangning Analytical Instrument Company, China) on the basis of the ISO5659-2 standard. The size of the sample was $75 \times 75 \times 2.5\ mm^3$, and the heat radiation was 25 kW m^{-2}. X-ray photoelectron spectrual (XPS) analysis was made with an Escalab spectrometer 250 apparatus (Thermo Scientific Ltd., U.S.) by using Al Kα excitation radiation of $h\nu = 1486.6$ eV.

3. Results and discussion

3.1. Characterization of prepared flame retardants

Fig. 1 shows the XRD spectra of different flame retardants. A (002) peak appearing at $2\theta = 25.1^\circ$can be seen in the spectrum of RGO, indicating a 0.35 nm interlayer spacing ($d_{(002)}$) of RGO. Compared with GO, the (002) peak of RGO has shifted to a larger angle, indicating the functional groups on the GO surface are no longer existent after reduction, forming RGO [22]. In addition, the XRD spectrum of ZIF-67 is consistent with previous literature and it has a good crystalline form [23]. In the XRD spectrum of MgAl-LDH, there are three characteristic peaks at $2\theta = 23.2^\circ$, 11.6°and 38.9°, respectively, corresponding to the diffraction peaks of LDH, and the interlamellar spacing of LDH can be calculated to be 0.76 nm according to the (003) peak, indicating that CO_3^{2-} exists in the interlayer of LDH [24]. What's more, the XRD spectrum of RGO-LDH is basically identical to that of LDH. The diffraction peak of RGO cannot be observed, which is attributed mainly to the lower content of RGO and the reduction of agglomeration for RGO [25]. Obviously,

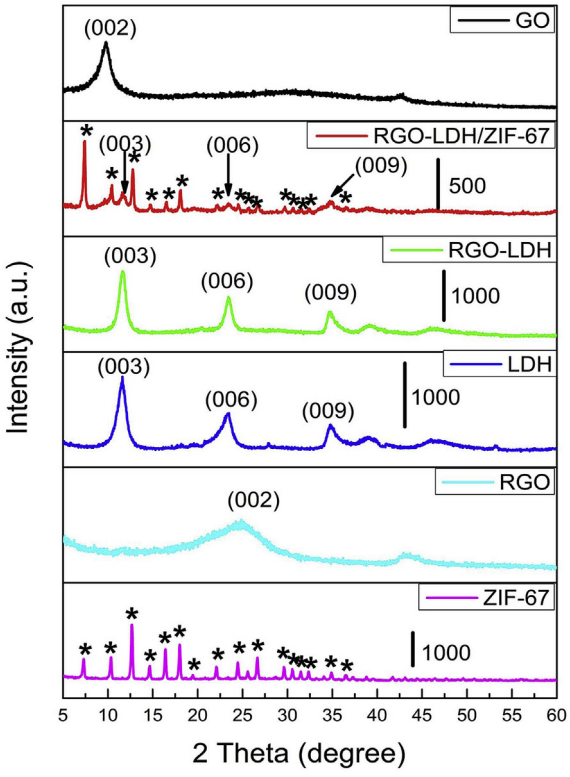

Fig. 1. XRD spectra of as-prepared samples.

Table 1
Formulas of neat EP and EP composites.

Samples	EP (wt%)	RGO (wt%)	LDH (wt%)	ZIF-67 (wt%)	RGO-LDH (wt%)	RGO-LDH/ZIF-67 (wt%)
EP0	100	0	0	0	0	0
EP1	98	2	0	0	0	0
EP2	98	0	2	0	0	0
EP3	98	0	0	2	0	0
EP4	98	0	0	0	2	0
EP5	98	0	0	0	0	2

the diffraction peaks of RGO-LDH and ZIF-67 are all evident (where "*" denotes the diffraction peak of ZIF-67) in the XRD spectrum of RGO-LDH/ZIF-67. The positions of (003), (006) and (009) peaks belonging to LDH are unchanged, indicating that ZIF-67 is satisfactorily grown on RGO-LDH, corresponding to the results of FTIR (Fig. S1).

TEM is usually used to visually observe the morphology of a material. Fig. 2 shows the TEM images of different flame retardants, and also the EDS spectrum of RGO-LDH/ZIF-67. As can be seen in Fig. 2 (a), the sheet of RGO is very thin and folded, which is attributed mainly to the Vander Waals' force and the π-π interaction between RGO layers that cause the stack of RGO layers. However, when LDH is grown on RGO, it is obvious that there are many sheet structures on RGO and the stacking phenomenon of RGO is improved, manifesting that LDH is firmly grown on RGO. On the basis of Fig. 2 (c) and (d), ZIF-67 appears on the surface of LDH. The main reason is that the surface oxygen-containing functional groups of GO are removed after their reduction so that ZIF-67 is no longer liable to react with RGO. Nevertheless, there is a certain amount of positive charges on LDH, and thus ZIF-67 can grow on the surface of LDH by electrostatic interaction.

3.2. Thermal behavior of prepared composites

Generally, the thermal properties of composite materials are very important in their applications. Fig. 3 displays the TGA and DTG results of prepared composites under air and nitrogen (the specific values are shown in Table 2). Specifically, $T_{10\%}$, denoting the initial decomposition temperature, shows the temperature when the mass loss of the composite material is 10%, and T_{max} shows the temperature when the decomposition rate of the composite material is at the maximum, and the char yield at 700 °C (CY) is found simultaneously.

As can be seen from Fig. 3 (a) and (b), the $T_{10\%}$ and T_{max} of pure EP under air are 388.3 °C and 395 °C, respectively. Obviously, the $T_{10\%}$ and T_{max} of the composites with different flame retardants are reduced to different extents, mainly because of the thermal conductivity of RGO and the catalytic effect of LDH and ZIF-67. However, the CY value of EP0 is merely 0.24% when the temperature reaches 700 °C. In comparison, the CY values of the composites are enhanced in varying degrees. Among them, the CY value of EP5 is 9.39%, which is the highest.

Fig. 3 (c) and (d) display the TGA results of EP and EP composites under nitrogen atmosphere, which show a different behavior for their thermal degradation because of the inert atmosphere. However, the $T_{10\%}$ and T_{max} of the EP composites with different flame retardants are also reduced compared with that of pure EP, which is attributed to the same reasons as under air. Obviously, the $T_{10\%}$ and T_{max} of pure EP are 397.5 °C and 425.0 °C, respectively, and the CY value of pure EP is 17.6%. Furthermore, compared with pure EP, the CY values of different EP composites are increased, indicating that the addition of flame retardants will form more char residue [26]. Particularly, the CY value of EP5 is 26.3%, which is the highest, indicating that RGO-LDH/ZIF-67 has the best effect in promoting char formation.

The glass transition temperature (Tg) is one of the characteristic temperatures of polymers, and is very important in their application. In this work, the Tg values of prepared composites is measured by DSC. The results are shown in Fig. S3. Evidently, the Tg values of the EP composites are increased in varying degrees against that of EP0, which is due mainly to the addition of inorganic flame retardants that would impede the movement of polymer segments to some extent.

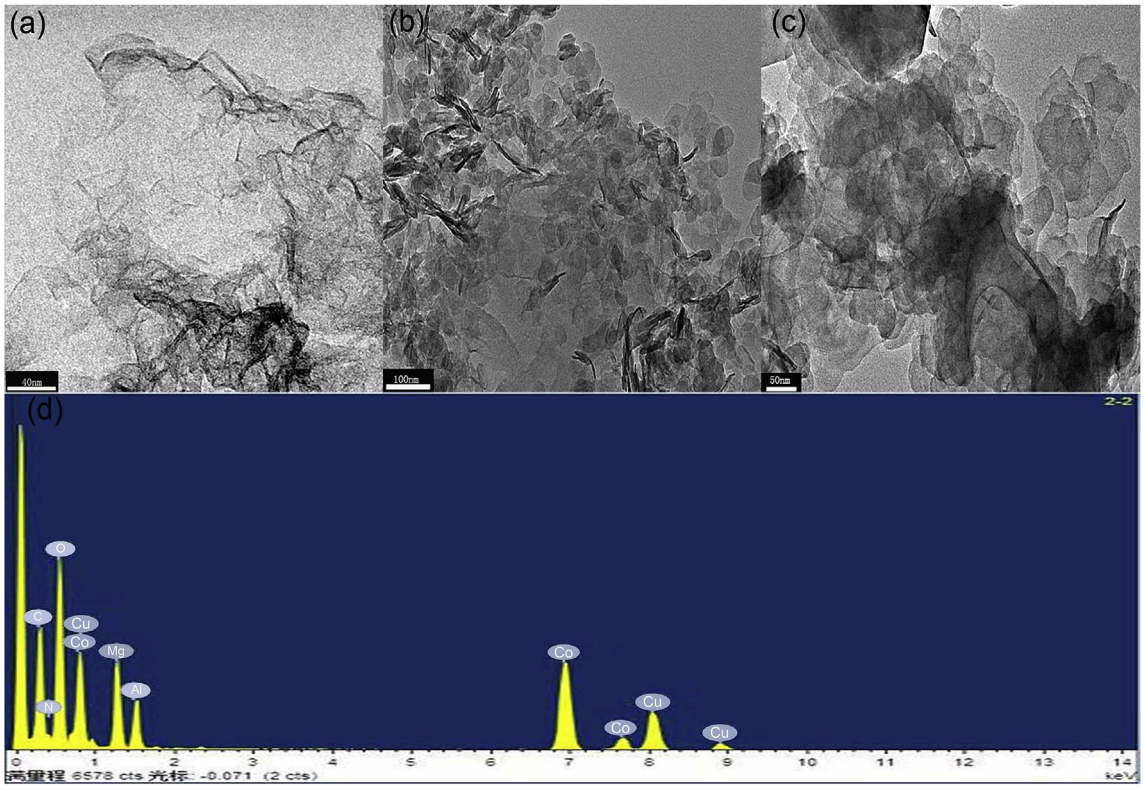

Fig. 2. TEM images of (a) RGO, (b) RGO-LDH, (c) RGO-LDH/ZIF-67 and EDS spectrum of (d) RGO-LDH/ZIF-67.

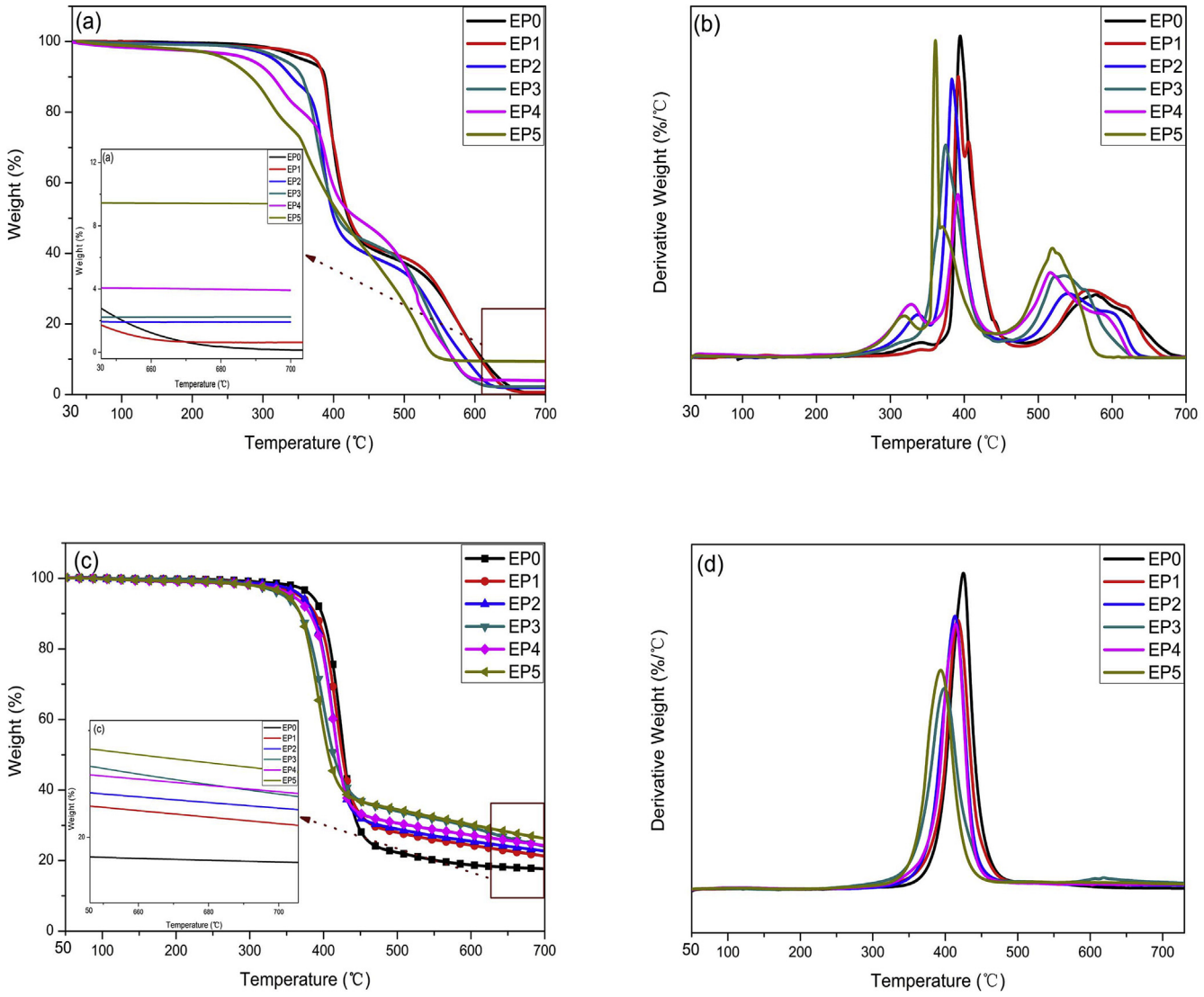

Fig. 3. TGA and DTG curves of neat EP and EP composites under (a), (b) air and (c), (d) nitrogen atmosphere.

Table 2
TGA data of neat EP and EP composites.

Sample	Air			Nitrogen		
	$T_{10\%}$ (°C)	T_{max} (°C)	CY (%)	$T_{10\%}$ (°C)	T_{max} (°C)	CY (%)
EP0	388.3	395.0	0.24	397.5	425.0	17.6
EP1	386.4	392.7	0.64	388.8	417.8	21.3
EP2	340.4	383.0	1.92	385.1	413.4	22.8
EP3	354.2	374.0	2.26	368.4	398.9	24.1
EP4	313.6	389.7	3.92	380.8	414.9	24.3
EP5	282.9	359.7	9.39	367.7	393.1	26.3

3.3. Flammability of prepared composites

The conical calorimeter test is a straightforward, rapid and valid way for measuring the combustion performance of polymers. The heat release rate is an important indicator to describe the fire risk of polymers, which can in turn help predict the behavior of polymers in practical combustion conditions. In addition, the char residue rate of polymers at a specific temperature can be measured by the mass change of polymers during the combustion process. Fig. 4 displays the heat release rate (HRR), total heat release (THR) and mass curves of different composites in the burning process (the specific values are displayed in Table 3). Obviously, the THR and peak heat release rate (PHRR) of EP0 are 58.6 MJ m^{-2} and 1355 kW m^{-2}, respectively, manifesting that EP0 is very inflammable in air and will release a lot of heat. However, compared to EP0, the THR and PHRR of the composites with different flame retardants are reduced. Among them, the THR and PHRR of EP5 decrease the most obviously, to 37.9 MJ m^{-2} and 464 kW m^{-2}, respectively, indicating that RGO-LDH/ZIF-67 has the best flame retardant effect. What's more, the char residue rate of EP5 with the combustion time of 260 s is increased from 10% to 17.9%. This is mainly because of the fact that RGO and LDH have a physical barrier effect and metal oxides may catalyze the generation of residue in the degradation of LDH and ZIF-67. At the same time, water vapor will be released in the burning process of LDH, lowering the temperature of polymer surface, and achieving a better flame retardant effect.

3.4. Smoke suppression of different composites

According to the results of the cone calorimeter test (by the ISO5660 standard), smoke release is also important in the

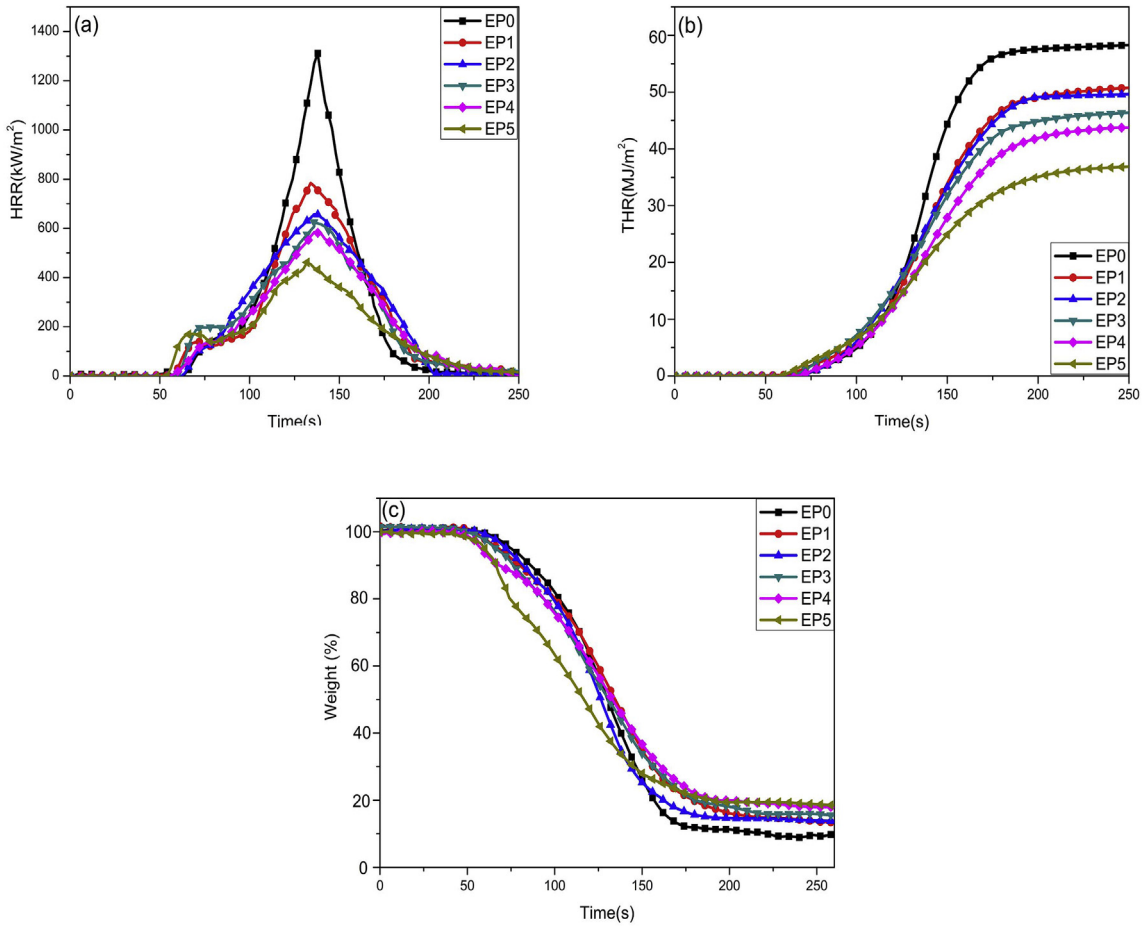

Fig. 4. HRR (a), THR (b) and weight loss(c) curves of neat EP and EP composites.

Table 3
Data from combustion tests of neat EP and EP composites.

Sample	PHRR ($kW \cdot m^{-2}$)	THR ($MJ \cdot m^{-2}$)	Weight (%)	SPR ($m^2 \cdot s^{-1}$)	TSP (m^2)	LOI (%)	$D_{s,max}$
EP0	1355	58.6	10.0	0.78	59.0	21.0	794.2
EP1	783	51.5	11.9	0.61	41.9	23.1	626.1
EP2	658	50.0	13.7	0.68	43.2	23.5	482.7
EP3	623	46.8	14.4	0.56	35.0	24.1	387.5
EP4	580	43.3	15.7	0.52	34.3	25.3	461.1
EP5	464	37.9	17.9	0.38	29.9	27.1	348.0

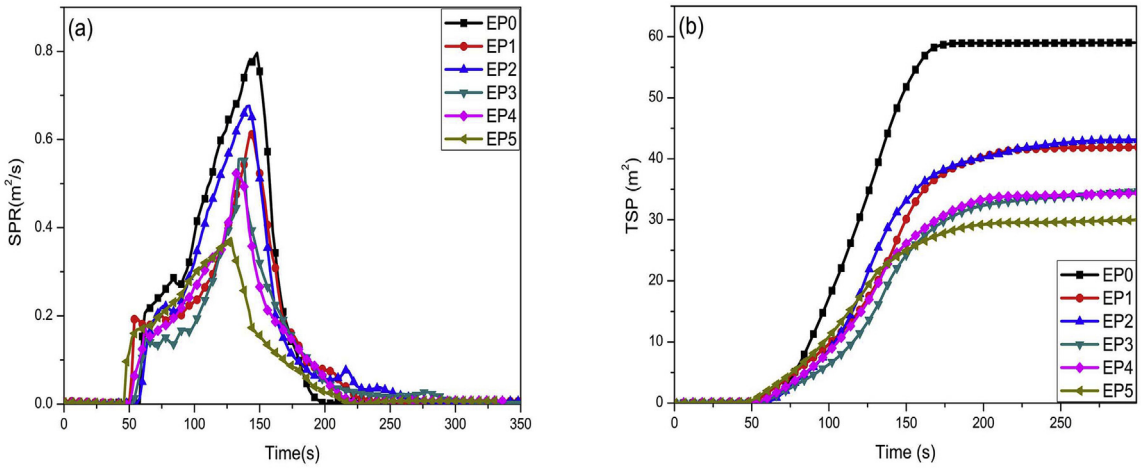

Fig. 5. SPR (a) and TSP (b) curves of EP composites.

burning process. Fig. 5 displays the smoke production rate (SPR) and total smoke production (TSP) curves of different composites (the specific values are displayed in Table 3). Clearly, the SPR and TSP of EP0 are 0.78 $m^2 s^{-1}$ and 59 m^2, respectively, indicating that heavy smoke will be released in the burning process of EP0. Compared with those of EP0, the SPR and TSP of EP composites with different flame retardants are reduced to varying degrees, and the SPR and TSP of EP5 are the lowest, at 0.38 $m^2 s^{-1}$ and 29.2 m^2, respectively. Obviously, RGO-LDH/ZIF-67 shows the best smoke suppression performance on EP compared with other flame retardants.

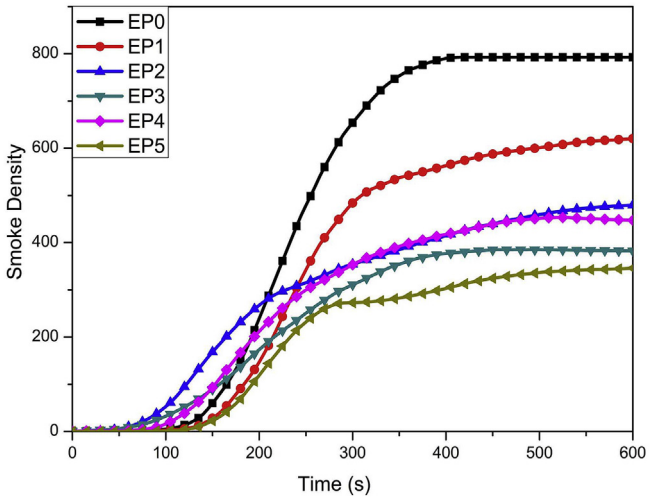

Fig. 6. Smoke density curves of pure EP and EP composites.

To fully illustrate the effect of RGO-LDH/ZIF-67 on the smoke suppression of EP, a flameless combustion test of the EP composites was carried out with a smoke density meter according to the ISO5659-2 standard. Fig. 6 shows the smoke situation of different composites (the specific values are displayed in Table 3). Evidently, the maximum smoke density ($D_{s,max}$) of EP0 is 794, indicating that EP0 will release a good deal of smoke when heated at high temperature. However, the $D_{s,max}$ of the EP composites with different flame retardants are decreased to some extent in comparison with EP0, especially that of EP5, which is decreased by 56.2%, demonstrating that RGO-LDH/ZIF-67 possesses the optimum efficiency in the smoke suppression effect. The above results reveal that the introduction of ZIF-67/LDH onto RGO can improve the smoke suppression effect of the composite effectively. This is due mainly to the physical barrier effect of RGO and LDH and the catalytic carbonization effect of the metal oxides formed in the degradation process of ZIF-67/LDH [10,27]. Furthermore, the mixed metal oxides with high surface area formed by decomposition of LDH at high temperature can absorb the acidic smoke to some extent [28], thus suppressing the smoke production more effectively.

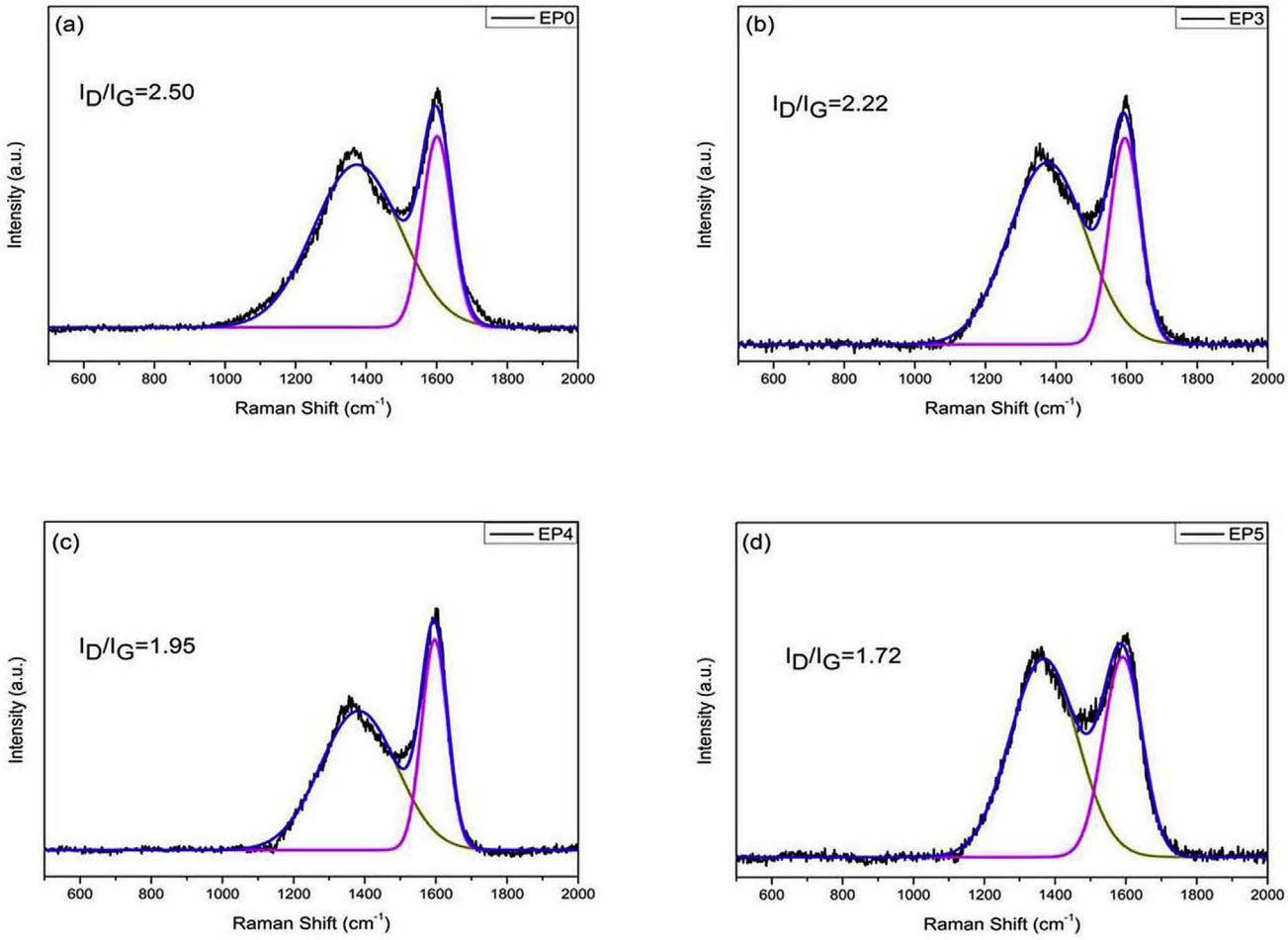

Fig. 7. Raman spectra of char residue of EP, EP3, EP4 and EP5 composites.

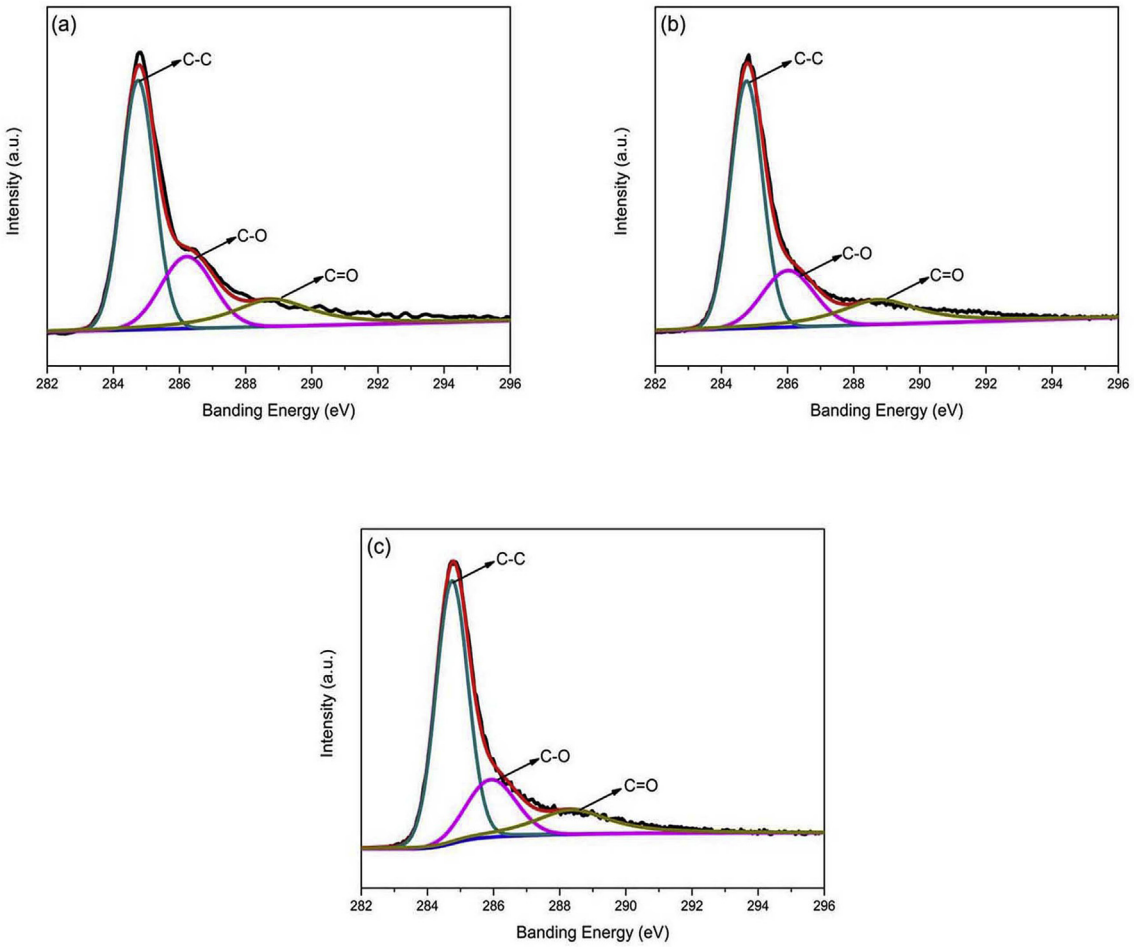

Fig. 8. C1s spectra of char residue of EP composites: (a) EP0 (b) EP4 (c) EP5.

3.5. Char analysis of different composites

The residual char generated after cone calorimeter burning of different composites is analyzed in order to effectively examine the fire retardant mechanism. Fig. 7 presents the Raman spectra of the residue of EP0, EP3, EP4 and EP5. Obviously, there are two strong peaks appearing at 1586 and 1354 cm^{-1}, agreeing with G and D bands. Usually, the higher the I_D/I_G (the intensity ratio of D and G band) value is, the lower the graphitization level of the residue, indicating that the char layer is less dense [29]. As can be seen from Fig. 7, the I_D/I_G value of EP0 is 2.50, while the I_D/I_G value of EP composite with 2 wt% RGO-LDH is lowered to 1.95, which is mainly because of the inhibition of RGO and LDH. In addition, metal oxides and water vapor will be generated with the degradation of LDH. Obviously, compared with that of EP4, the I_D/I_G value of EP5 is further reduced, indicating that the residue of EP5 produces the highest graphitization level, and its residue is the densest. This is due mainly to the formation of Co_3O_4 in the combustion process of ZIF-67, and Co_3O_4 promotes the generation of dense residue.

The char layer formed after the conical calorimeter test is also analyzed by XPS. Fig. 8 displays the C1s spectra of the residue of EP0, EP4 and EP5 after the conical calorimeter test. The specific values are shown in Table S1. As can be seen from Fig. 8, there are three peaks appearing at 284.6 (C-C), 285.8 (C-O) and 287.4 (C=O) eV, respectively [30]. In general, the ratio between the oxidation carbon Cox and the nonoxidation carbon Ca may be used to evaluate the thermal oxidation properties of materials: the larger the Cox/Ca value is, the easier the oxidation for the materials, indicating the thermal oxidation performance of these materials is less satisfactory [30]. It can be seen from Fig. 8 and Table S1 that the Cox/Ca values of EP0, EP4 and EP5 are 0.83, 0.71 and 0.62, respectively, indicating that pure EP has poor thermal oxidation resistance. Obviously, the thermal oxidation resistance of the composites with different flame retardants is improved. With 2 wt% RGO-LDH/ZIF-67 added, the thermal oxidation resistance of the EP composites is the best, indicating that RGO-LDH/ZIF-67 can effectively improve the thermal oxidation resistance of polymer materials.

Fig. 9 shows the Co2p and XRD spectra of the char layers of EP5 after the conical calorimeter test. Two peaks can be clearly seen in Fig. 9 (a) at 780.5 and 796.2 eV, respectively, corresponding to $Co2p^{3/2}$ and $Co2p^{1/2}$, indicating the existence of Co_3O_4. In addition, the peaks existing in 785.6 and 802.1 eV correspond to the satellites of Co_3O_4 [31]. According to the above results, Co_3O_4 is formed in the burning process of EP5 and it would facilitate the generation of residue. Therefore, RGO-LDH/ZIF-67 can reduce the fire hazard of EP effectively. What's more, these results can be further proved according to the XRD spectra of the char layers of EP5 [32].

4. Conclusions

In this study, different flame retardants were fabricated with a simple method, then the prepared samples were added into EP by physical blending, and their effects on the thermal behavior, flame

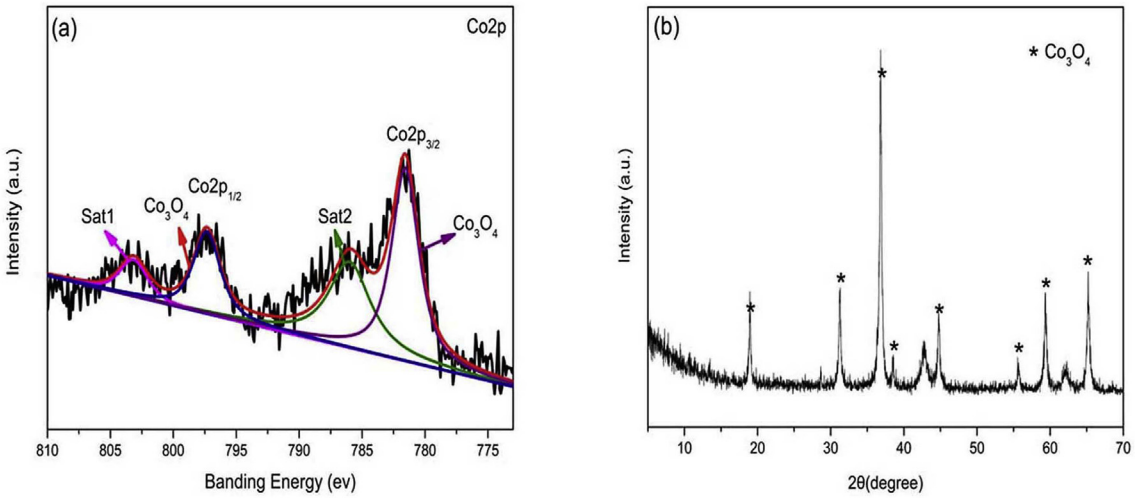

Fig. 9. Co2p and XRD spectra of char residue of EP5.

retardant and smoke suppression properties of EP were studied. According to the results of the thermal property analysis, the residual rate (700 °C) and the Tg values of the EP composites were improved to different extents in comparison with EP0. What's more, the residual rate of the composite with 2 wt% RGO-LDH/ZIF-67 was increased obviously under nitrogen, reaching 26.3%. The results of various combustion tests showed that RGO-LDH/ZIF-67 had the most conspicuous effect on improving the flame retardant and smoke suppression properties of EP. The reduced fire risk of the composite was due mainly to the physical barrier effect of RGO and LDH and the catalytic carbonization effect of RGO-LDH/ZIF-67. In addition, the water vapor generated in the combustion process of LDH reduced the surface temperature of polymers, thus preventing the polymer from burning. Furthermore, the results of char analysis revealed that the graphitization level and thermal oxidation property of the char residue were improved with the incorporation of ZIF-67.

Acknowledgements

The authors express their gratitude to the Anhui Provincial Natural Sciencs Foundation (1708085ME113), the Natural Science Research Project of Colleges and Universities in Anhui Province (KJ2018A0522) and Polymer Materials and Engineering Specialty Comprehensive Reform Pilot Project in College Quality Engineering Project of Anhui Province (2016zy031) for their support.

Appendix A. Supplementary data

Supplementary data related to this article can be found at https://doi.org/10.1016/j.polymdegradstab.2018.05.022.

References

[1] P. Müller, M. Morys, A. Sut, C. Jäger, B. Illerhaus, B. Schartel, Melamine poly(zinc phosphate) as flame retardant in epoxy resin: decomposition pathways, molecular mechanisms and morphology of fire residues, Polym. Degrad. Stabil. 130 (2016) 307–319.
[2] Q.H. Kong, T. Wu, J.H. Zhang, D.Y. Wang, Simultaneously improving flame retardancy and dynamic mechanical properties of epoxy resin nanocomposites through layered copper phenylphosphate, Compos. Sci. Technol. 154 (2018) 136–144.
[3] M. Dogan, S.M. Unlu, Flame retardant effect of boron compounds on red phosphorus containing epoxy resins, Polym. Degrad. Stabil. 99 (2014) 12–17.
[4] S.J. Wang, F. Xin, Y. Chen, L.J. Qian, Y.J. Chen, Phosphorus-nitrogen containing polymer wrapped carbon nanotubes and their flame-retardant effect on epoxy resin, Polym. Degrad. Stabil. 129 (2016) 133–141.
[5] S. Ullah, F. Ahmad, Effects of zirconium silicate reinforcement on expandable graphite based intumescent fire retardant coating, Polym. Degrad. Stabil. 103 (2014) 49–62.
[6] W. Cai, J.L. Wang, Y. Pan, W.W. Guo, X.W. Mu, X.M. Feng, et al., Mussel-inspired functionalization of electrochemically exfoliated graphene: based on self-polymerization of dopamine and its suppression effect on the fire hazards and smoke toxicity of thermoplastic polyurethane, J. Hazard Mater. 352 (2018) 57–69.
[7] B.H. Yuan, A. Fan, M. Yang, X.F. Chen, Y. Hu, C.L. Bao, et al., The effects of graphene on the flammability and fire behavior of intumescent flame retardant polypropylene composites at different flame scenarios, Polym. Degrad. Stabil. 143 (2017) 42–56.
[8] B. Dittrich, K.A. Wartig, R. Mülhaupt, B. Schartel, Flame-retardancy properties of intumescent ammonium poly(phosphate) and mineral filler magnesium hydroxide in combination with graphene, Polymers 6 (2014) 2875–2895.
[9] B. Dittrich, K.A. Wartig, D. Hofmann, R. Mülhaupt, B. Schartel, Flame retardancy through carbon nanomaterials: carbon black, multiwall nanotubes, expanded graphite, multi-layer graphene and graphene in polypropylene, Polym. Degrad. Stabil. 98 (2013) 1495–1505.
[10] F. Sun, T. Yu, C.Q. Hu, Y. Li, Influence of functionalized graphene by grafted phosphorus containing flame retardant on the flammability of carbon fiber/epoxy resin (CF/ER) composite, Compos. Sci. Technol. 136 (2016) 76–84.
[11] N.F. Attia, N.S.A. El-Aal, M.A. Hassan, Facile synthesis of graphene sheets decorated nanoparticles and flammability of their polymer nanocomposites, Polym. Degrad. Stabil. 126 (2016) 65–74.
[12] B.H. Yuan, Y. Hu, X.F. Chen, Y.Q. Shi, Y. Niu, Y. Zhang, et al., Dual modification of graphene by polymeric flame retardant and $Ni(OH)_2$ nanosheets for improving flame retardancy of polypropylene, Composer Part A 100 (2017) 106–117.
[13] N.F. Attia, N.S.A. El-Aal, M.A. Hassan, Facile synthesis of graphene sheets decorated nanoparticles and flammability of their polymer nanocomposites, Polym. Degrad. Stabil. 126 (2016) 65–74.
[14] Y.X. Yan, H.B. Yao, L.B. Mao, A.M. Asiri, K.A. Alamry, H.M. Marwaini, S.H. Yu, Micrometer-thick graphene oxide-layered double hydroxide nacre-inspired coatings and their properties, Small 12 (2016) 745–755.
[15] D.Y. Wang, A. Leuteritz, Y.Z. Wang, U. Wagenknecht, G. Heinrich, Preparation and burning behaviors of flame retarding biodegradable poly(lactic acid) nanocomposite based on zinc aluminum layered double hydroxide, Polym. Degrad. Stabil. 95 (2010) 2474–2480.
[16] H. Li, S. Yao, H.L. Wu, J.Y. Qu, Z.M. Zhang, T.B. Lu, W.B. Lin, E.B. Wang, Charge-regulated sequential adsorption of anionic catalysts and cationic photosensitizers into metal-organic frameworks enhances photocatalytic proton reduction, Appl. Catal., B 224 (2018) 46–52.
[17] R. Abazari, A.R. Mahjoub, Ultrasound-assisted synthesis of Zinc(II)-based metal organic framework nanoparticles in the presence of modulator for adsorption enhancement of 2,4-dichlorophenol and amoxicillin, Ultrason. Sonochem. 42 (2018) 577–584.
[18] L. Garzón-Tovar, J. Pérez-Carvajal, I. Imaz, D. Maspoch, Composite salt in porous metal-organic frameworks for adsorption heat transformation, Adv. Funct. Mater. 27 (2017) 1–10.
[19] T.T. Ma, C.G. Guo, Synergistic effect between melamine cyanurate and a novel flame retardant curing agent containing a caged bicyclic phosphate on flame retardancy and thermal behavior of epoxy resins, J. Anal. Appl. Pyrol. 124 (2017) 239–246.
[20] S.L. Qiu, W.Y. Xing, X.M. Feng, B. Yu, X.W. Mu, R.K.K. Yuen, Y. Hu, Self-standing

cuprous oxide nanoparticles on silica@polyphosphazene nanospheres: 3D nanostructure for enhancing the flame retardancy and toxic effluents elimination of epoxy resins via synergistic catalytic effect, Chem. Eng. J. 309 (2016) 802–814.
[21] M.R. Nabid, Y. Bide, N. Fereidouni, B. Etemadi, Maghemite/nitrogen-doped graphene hybrid material as a reusable bifunctional catalyst for glycolysis of polyethylene terephthalate, Polym. Degrad. Stabil. 144 (2017) 434–441.
[22] M. Sedki, R.Y.A. Hassan, A. Hefnawy, I.M. El-Sherbiny, Sensing of bacterial cell viability using nanostructured bioelectrochemical system: rGO-hyperbranched chitosan nanocomposite as a novel microbial sensor platform, Sensor. Actuator. B Chem. 252 (2017) 191–200.
[23] M. Ammar, S. Jiang, S.F. Ji, Heteropoly acid encapsulated into zeolite imidazolate framework (ZIF-67) cage as an efficient heterogeneous catalyst for Friedel–Crafts acylation, J. Solid State Chem. 233 (2016) 303–310.
[24] R.R. Shan, L.G. Yan, Y.M. Yang, K. Yang, S.J. Yu, H.Q. Yu, B.C. Zhu, B. Din, Highly efficient removal of three red dyes by adsorption onto Mg-Al-layered double hydroxide, J. Ind. Eng. Chem. 21 (2015) 561–568.
[25] P. Thangaraj, M.R. Viswanathan, K. Balasubramanian, H.D. Mansilla, D. Contreras, S.S. Guzman, M.A.G. Pinilla, Ultrasound assisted synthesis of morphology tunable rGO: ZnO hybrid nanostructures and their optical and UV-A light driven photocatalysis, J. Lumin. 186 (2017) 53–61.
[26] B. Zhao, W.J. Liang, J.S. Wang, F. Li, Y.Q. Liu, Synthesis of a novel bridged-cyclotriphosphazene flame retardant and its application in epoxy resin, Polym. Degrad. Stabil. 133 (2016) 162–173.
[27] Q.H. Kong, T. Wu, H.K. Zhang, Y. Zhang, M.M. Zhang, T.Y. Si, L. Yang, J.H. Zhang, Improving flame retardancy of IFR/PP composites through the synergistic effect of organic montmorillonite intercalation cobalt hydroxides modified by acidified chitosan, Appl. Clay Sci. 146 (2017) 230–237.
[28] S.L. Xu, L.X. Zhang, Y.J. Lin, R. Li, F.Z. Zhang, Layered double hydroxides used as flame retardant for engineering plastic acrylonitrile-butadiene-styrene (ABS), J. Phys. Chem. Solid. 73 (2012) 1514–1517.
[29] W. Cai, X.M. Feng, B.B. Wang, W.Z. Hu, B.H. Yuan, N.N. Hong, Y. Hu, A novel strategy to simultaneously electrochemically prepare and functionalize graphene with a multifunctional flame retardant, Chem. Eng. J. 316 (2017) 514–524.
[30] W.Z. Xu, S.Q. Wang, A.J. Li, X.L. Wang, Synthesis of aminopropyltriethoxysilane grafted/tripolyphosphate intercalated ZnAl LDHs and its performance in the flame retardancy and smoke suppression of polyurethane elastomer, RSC Adv. 6 (2016) 48189–48198.
[31] C.Y. Song, D.M. Zhang, K. Ye, W. Zeng, X.Y. Yang, Y.Z. Wang, Y.C. Shen, D.X. Cao, K. Cheng, G.L. Wang, In-situ reduced petal-like cobalt on Ni foam based cobaltosic oxide as an efficient catalyst for hydrogen peroxide electroreduction, J. Electroanal. Chem. 788 (2017) 74–82.
[32] E. Zhang, Y. Xie, S.Q. Ci, J.C. Jia, Z.H. Wen, Porous Co_3O_4 hollow nanododecahedra for nonenzymatic glucose biosensor and biofuel cell, Biosens. Bioelectron. 81 (2016) 46–53.